Chiral Domain-Wall States in a Quadratic Hamiltonian

Tetsuyuki OCHIAI

Photonic Materials Unit, National Institute for Materials Science (NIMS), Tsukuba, Ibaraki 305-0044, Japan

In two-dimensional lattice systems, the effective Hamiltonian around a doubly degenerate point at the Brillouin-zone center can be of a similar form to the d-wave Bogoliubov-Nambu Hamiltonian. A band gap opens there if a perturbation of time-reversal-symmetry breaking is introduced. In such a system, two domain-wall states with the same chirality emerge around the interface between two domains having the gap parameters of opposite signs. The domain-wall states have asymptotically quadratic dispersions, in contrast to the domain-wall state of the Dirac fermion, which has a linear dispersion irrespective of the domain-wall profile. As an explicit example, we numerically study the domain-wall states of photons in a honeycomb-lattice photonic crystal. The results are in agreement with those obtained using the effective theory based on the quadratic Hamiltonian.

1. Introduction

A domain wall and a localized state in it are universal items that many physical systems have in common. In the lattice gauge theory, for instance, a domain wall in fictitious five-dimensional space-time provides a means of constructing chiral fermions on a four-dimensional space-time lattice.[1] In condensed-matter systems, a domain-wall state emerges realistically. It is sometimes the case that a low-energy excitation of a two-dimensional (2d) electron system is described by massive Dirac fermions.[2] The mass term is supposed to be controllable by some means. If the system consists of two domains that are in contact with each other, then a domain-wall state with a linear dispersion emerges, provided that the mass terms have opposite signs in the two domains.[3] This is the so-called domain-wall fermion, which is chiral in the sense that it propagates unidirectionally.

The key point here is the sign of the mass, because it is closely related to topology. The Chern number C of the Dirac fermion, which represents the vorticity in momentum space, corresponds to $1/2\times\mathrm{sgn}(M)$, where M is the mass of the Dirac fermion.[4] The Chern number in the bulk is directly related to a possible edge mode as a consequence of the so-called bulk-edge correspondence.[5] It states that the number of possible interface states localized in the domain wall is given by the difference in the Chern number between the two domains, which is equal to 1 if the masses have opposite signs.

As described above, domain-wall states are often argued in the context of the Dirac Hamiltonian for fermions. However, even if the Dirac Hamiltonian is not applicable, or even if an effective Hamiltonian is given for bosons, it is possible to obtain domain-wall states with chirality. Here, we use the term "chirality" as in quantum Hall systems. Namely, "chiral" states refer to those propagating unidirectionally. A landmark in this context is the realization of chiral domain-wall states of photons using photonic Dirac cones.[6] Here, we present another nontrivial example found in a quadratic Hamiltonian. The presence of such a state was already suggested in 2d square photonic crystals (PhCs) with a broken time-reversal symmetry (TRS).[7,8] However, an explicit derivation of domain-wall states, in a detailed comparison between a first-principles calculation and an effective Hamiltonian, is still lacking.

In this paper, we derive an effective Hamiltonian applicable to both bosons and fermions, from the viewpoint of the group theory. Under certain conditions for the underlying lattice structure, a quadratic Hamiltonian is derived around the Brillouin zone (BZ) center of lattice systems. Such a Hamiltonian has a similar form to the d-wave Bogoliubov-Nambu Hamiltonian,[9] and can have a nontrivial topology of the eigenstates in momentum space. Thus, the present study sheds light on topological superconductors[10,11] from a different angle. Next, we study domain-wall states based on an effective quadratic Hamiltonian. Under certain conditions, two domain-wall states emerge, and are shown to be chiral. We also show that their asymptotic forms in dispersion curves coincide to the band edges of a bulk band structure.

Taking the honeycomb-lattice PhC as a nontrivial example, we numerically consider domain-wall states of photons on the basis of the effective Hamiltonian around the BZ center. The results are in good agreement with those obtained by first-principles calculation of the PhC. The first-principles calculation also highlights the edge states of open boundaries. They exhibit marked contrast to domain-wall states in terms of properties, but are also chiral.

One reason why such an effective Hamiltonian has not been investigated well is the compatibility between the translational invariance of lattice systems and a TRS-breaking perturbation. In conventional electronic systems, a TRS-breaking perturbation such as a nonzero external magnetic field destroys a simple lattice-translational invariance. An extra Peierls phase (Aharonov-Bohm phase) is accompanied by lattice translation. As a result, the Bloch momentum inherent in lattice systems loses its original meaning. Accordingly, the $\boldsymbol{k}\cdot\boldsymbol{p}$ perturbation does not work under the TRS-breaking perturbation. One way to avoid the incompatibility is to introduce a periodic magnetic field having zero flux per unit cell (UC). In striking contrast, optics is free from such incompatibility, because a photon is a neutral particle and thus no Peierls phase is involved. Therefore, such an effective Hamiltonian with a nontrivial topology is easily obtained.

This paper is organized as follows. In §2, we derive an effective quadratic Hamiltonian from the viewpoint of the group theory. In §3, domain-wall states are analyzed on the basis of

the effective Hamiltonian. In §4, we present an explicit example of domain-wall states for photons using honeycomb-lattice photonic structures. Both the first-principles calculation and the effective-Hamiltonian calculation are employed, and their results are compared. The conclusion is given in §5. In Appendix A, two physical systems showing effective quadratic Hamiltonians are presented. In Appendix B, a group-theoretical argument is given in a model-independent manner, to determine possible forms of the quadratic Hamiltonians.

2. Effective Quadratic Hamiltonian around Brillouin-Zone Center

First, let us define the effective Hamiltonian under consideration:

$$\mathcal{H} = \lambda_1|\boldsymbol{k}|^2\hat{1} + \lambda_2[(k_x^2 - k_y^2)\sigma_3 + 2k_xk_y\sigma_1] + \Lambda_\zeta\sigma_2, \quad (1)$$

where $\hat{1}$ is the 2×2 unit matrix, and σ_i ($i = 1, 2, 3$) is the Pauli matrix. The eigenvalues of the Hamiltonian are given by

$$\mathcal{E}_\pm = \lambda_1|\boldsymbol{k}|^2 \pm \sqrt{\lambda_2^2|\boldsymbol{k}|^4 + \Lambda_\zeta^2}. \quad (2)$$

Here, the parameter Λ_ζ corresponds to the gap at $\boldsymbol{k} = 0$, and has profound importance from the viewpoint of topology, as we will see later. Such a Hamiltonian with a vanishing Λ_ζ emerges in triangular-, honeycomb-, and kagome-lattice systems with the C_{6v} point group. If we allow a difference in weight between $(k_x^2-k_y^2)\sigma_3$ and $2k_xk_y\sigma_1$, it includes the square lattice with the C_{4v} point group.[8] The honeycomb lattice with the C_{3v} point group results in the effective Hamiltonian of Eq. (1) plus an additional term given by

$$\Delta\mathcal{H} = \Lambda_{k\zeta}(k_x\sigma_3 - k_y\sigma_1). \quad (3)$$

This term represents the anisotropy in momentum space.

The above point groups allow for 2d irreducible representations (IRRs), resulting in a doubly degenerate eigenmode at the BZ center (Γ point). In fact, it is quite common for a lattice system having one of the point groups to exhibit two quadratic curves touching each other at $\boldsymbol{k} = 0$. We can show by the $\boldsymbol{k}\cdot\boldsymbol{p}$ perturbation that such curves are derived using the effective Hamiltonian of the degenerate perturbation theory. In addition, a nonzero Λ_ζ can be explained by the first-order perturbation of broken TRS. The derivation of the effective Hamiltonian is given as follows (further details can be found in Appendices).

Suppose that the full Hamiltonian to be diagonalized is composed of the $\mathcal{G}$-symmetric part H_0 and the perturbation H_1. Here, $\mathcal{G}$ refers to the point group listed above. The zeroth order Hamiltonian H_0 is for $\boldsymbol{k} = \boldsymbol{0}$ and can be solved, at least numerically. The perturbation H_1 includes the terms of the nonzero $\boldsymbol{k}$ and the TRS-breaking one parametrized by ζ ($\zeta = 0$ corresponds to the vanishing perturbation). The eigenstates of H_0 are classified according to the IRRs of $\mathcal{G}$. We start with a doubly degenerate mode whose eigenvalue and eigenvectors are denoted as $E_0^{(0)}$ and $|\psi_0^{(0p)}\rangle$ $(p = 1, 2)$, respectively. The other modes are denoted as $E_0^{(n)}$ and $|\psi_0^{(n)}\rangle$. Then, the effective Hamiltonian for the degenerate mode in the Lödwin perturbation scheme is given by

$$\mathcal{H}_{pq} = \langle\psi_0^{(0p)}|H'|\psi_0^{(0q)}\rangle + \sum_{n\neq0}\frac{\langle\psi_0^{(0p)}|H'|\psi_0^{(n)}\rangle\langle\psi_0^{(n)}|H'|\psi_0^{(0q)}\rangle}{E_0^{(0)} - E_0^{(n)}} + \cdots. \quad (4)$$

We collect terms up to the second order in $\boldsymbol{k}$ and ζ. Generally, the first- and second-order terms in $\boldsymbol{k}$ satisfy

$$\mathcal{H}^{(k)}(\boldsymbol{k}) = D_R^\dagger(A)\mathcal{H}^{(k)}(A\boldsymbol{k})D_R(A), \quad (5)$$

$$\mathcal{H}^{(k^2)}(\boldsymbol{k}) = D_R^\dagger(A)\mathcal{H}^{(k^2)}(A\boldsymbol{k})D_R(A), \quad (6)$$

where R stands for the IRR of the doubly degenerate mode concerned, A is an element of $\mathcal{G}$, and $D_R(A)$ is a unitary representation of A. Similarly, the first- and second-order terms in ζ and the cross term in $\boldsymbol{k}$ and ζ satisfy

$$\mathcal{H}^{(\zeta)} = \det A^{-1}D_R^\dagger(A)\mathcal{H}^{(\zeta)}D_R(A), \quad (7)$$

$$\mathcal{H}^{(\zeta^2)} = D_R^\dagger(A)\mathcal{H}^{(\zeta^2)}D_R(A), \quad (8)$$

$$\mathcal{H}^{(k\zeta)}(\boldsymbol{k}) = \det A^{-1}D_R^\dagger(A)\mathcal{H}^{(k\zeta)}(A\boldsymbol{k})D_R(A). \quad (9)$$

The above symmetry properties can be verified, for instance, with a nonrelativistic electron under a periodic potential and a periodic magnetic field with zero flux per UC (see Appendix A.1):

$$H = \frac{1}{2m}(\boldsymbol{p} + e\boldsymbol{A}(\boldsymbol{x}))^2 + V(\boldsymbol{x}), \quad (10)$$

$$\boldsymbol{A}(\boldsymbol{x}+\boldsymbol{a}) = \boldsymbol{A}(\boldsymbol{x}), \quad V(\boldsymbol{x}+\boldsymbol{a}) = V(\boldsymbol{x}), \quad (11)$$

or its tight-binding model analog proposed by Haldane.[12] Here, $\boldsymbol{a}$ is an elementary lattice vector. If a uniform magnetic field is employed, the momentum $\boldsymbol{k}$ is no longer a good quantum number.[13] Thus, the above perturbation scheme does not work.

These constraints on the effective Hamiltonian enable us to derive its possible forms. The results are summarized as follows (see Appendix B):

$$\mathcal{H}^{(k)} = 0, \quad (12)$$

$$\mathcal{H}^{(k^2)} = \begin{cases} c_1|\boldsymbol{k}|^2\hat{1} + c_2[(k_x^2 - k_y^2)\sigma_3 + 2k_xk_y\sigma_1] \\ (C_{3v}, C_{6v}) \\ c_1|\boldsymbol{k}|^2\hat{1} + c_2(k_x^2 - k_y^2)\sigma_3 + c_3 2k_xk_y\sigma_1 \\ (C_{4v}) \end{cases}, \quad (13)$$

$$\mathcal{H}^{(\zeta)} \propto \sigma_2, \quad (14)$$

$$\mathcal{H}^{(\zeta^2)} \propto \hat{1}, \quad (15)$$

$$\mathcal{H}^{(k\zeta)} \propto \begin{cases} k_x\sigma_3 - k_y\sigma_1 & (C_{3v}) \\ 0 & (C_{4v}, C_{6v}) \end{cases}. \quad (16)$$

Summing up all the terms, we obtain Eqs. (1) and (3).

Using the effective Hamiltonian, we can study the topological properties of the eigenstates in momentum space. They are characterized by the Berry phase or its variants, i.e., the Berry curvature and Chern number. The Berry phase θ_B of the eigenstate for a closed circle in momentum space is defined by[14]

$$\theta_B = \oint \mathrm{d}\boldsymbol{k}\cdot\boldsymbol{A}_{\boldsymbol{k}}, \quad (17)$$

$$\boldsymbol{A}_{\boldsymbol{k}} = \mathrm{i}\langle\psi|\boldsymbol{\nabla}_{\boldsymbol{k}}|\psi\rangle, \quad (18)$$

where $\boldsymbol{\nabla}_{\boldsymbol{k}}$ is the gradient operator with respect to $\boldsymbol{k}$. By the diagonalization of the effective Hamiltonian, the Berry phase

of the eigenstate is evaluated as

$$\theta_B = \pm 2\pi \mathrm{sgn}(\Lambda_\zeta), \tag{19}$$

for the upper (minus sign) and lower (plus sign) bands,[8,15] provided that the circle radius is small enough with respect to $|\Lambda_\zeta|$. This phase suggests that the Chern number of the relevant bands becomes $\pm\mathrm{sgn}(\Lambda_\zeta)$. However, it is sometimes the case that, in an unperturbed system, the two bands under consideration touch other bands at different points in the first BZ. This happens for the square lattice with C_{4v} and the triangular, honeycomb, and kagome lattices with C_{6v} at a BZ corner. In such cases, the topology of relevant bands is affected by the BZ corner. Thus, the above estimation of the Chern number will be modified.

In this way, we see that the parameter Λ_ζ has profound importance. It is remarkable that this parameter represents the degree of TRS breaking of the system. Furthermore, in some cases, it is controllable by applying an external magnetic field (see Appendix A). For instance, if the magnetic field is inverted, Λ_ζ changes its sign, resulting in a topology change of the eigenstates in momentum space. This property gives rise to novel domain-wall states in a controllable manner.

3. Domain-Wall States

Once we have an effective quadratic Hamiltonian for the bulk system with the controllable gap parameter Λ_ζ, we can set up a domain wall formed by two domains having the gap parameters of opposite signs. One way to realize the domain wall is to employ antiparallel magnetic fields between two domains in a magneto-optical PhC, as we will see in §5. Such a domain wall may be physically interesting, because it can be a platform of novel interface phenomena. As for the Dirac Hamiltonian, a novel domain-wall state emerges, if the Dirac mass parameters of the two domains have opposite signs. The resulting domain-wall state, which is sometimes called the "zero mode",[3] has a linear and gapless dispersion irrespective of system details. Its condensed-matter realization has been discussed recently within the context of topological insulators and topological superconductors.[16] Here, we should emphasize that, even for the quadratic Hamiltonian discussed in §2, we can show that similar zero modes emerge in the domain wall.

Let us consider the effective Hamiltonian for a domain-wall system. We assume that the system has two domains with gap parameters Λ_ζ of opposite signs. To be specific, suppose that the two domains are separated at approximately $y = 0$ with the following profiles of the gap parameter: $\Lambda_\zeta(y) \to \Lambda_- < 0$ ($y \to -\infty$) and $\Lambda_\zeta(y) \to \Lambda_+ > 0$ ($y \to \infty$). The relevant Hamiltonian now becomes

$$\mathcal{H} = \lambda_1 \left(k_x^2 - \frac{\partial^2}{\partial y^2}\right)\hat{1} + \lambda_2 \left[\left(k_x^2 + \frac{\partial^2}{\partial y^2}\right)\sigma_3 - 2\mathrm{i}k_x \frac{\partial}{\partial y}\sigma_1\right] + \Lambda_\zeta(y)\sigma_2, \tag{20}$$

simply replacing k_y in Eq. (1), with the momentum operator $-\mathrm{i}\partial/\partial y$.

To analyze possible domain-wall states, we neglect the quadratic derivative terms in the eigenvalue equation

$$\mathcal{H}\psi = \mathcal{E}\psi. \tag{21}$$

The validity of the assumption is discussed immediately after the analytical derivation given below. Then, the equation becomes

$$-2\mathrm{i}\lambda_2 k_x \frac{\partial v}{\partial y} - \mathrm{i}\Lambda_\zeta(y)v \simeq [\mathcal{E} - (\lambda_1 + \lambda_2)k_x^2]u, \tag{22}$$

$$-2\mathrm{i}\lambda_2 k_x \frac{\partial u}{\partial y} + \mathrm{i}\Lambda_\zeta(y)u \simeq [\mathcal{E} - (\lambda_1 - \lambda_2)k_x^2]v, \tag{23}$$

for the two-component eigenvector $\psi = (u, v)^t$. This equation has a zero mode:

$$\psi = \begin{pmatrix} 0 \\ 1 \end{pmatrix} \mathrm{e}^{-\frac{1}{2\lambda_2 k_x}\int^y dy' \Lambda_\zeta(y')}, \tag{24}$$

with the spectrum $\mathcal{E} = (\lambda_1 - \lambda_2)k_x^2$ if $\lambda_2 k_x > 0$. Similarly, if $\lambda_2 k_x < 0$, the equation has another zero mode:

$$\psi = \begin{pmatrix} 1 \\ 0 \end{pmatrix} \mathrm{e}^{\frac{1}{2\lambda_2 k_x}\int^y dy' \Lambda_\zeta(y')}, \tag{25}$$

with the spectrum $\mathcal{E} = (\lambda_1 + \lambda_2)k_x^2$. These zero modes are confined around the domain wall. The localization length L is evaluated as $L \simeq |2\lambda_2 k_x/\Lambda_\pm|$.

To justify the assumption of neglecting the second derivative with respect to y, we must have

$$\left|\pm\frac{1}{2\lambda_2 k_x}\frac{\partial \Lambda_\zeta}{\partial y} + \left(\frac{\Lambda_\zeta}{2\lambda_2 k_x}\right)^2\right| \ll k_x^2. \tag{26}$$

Therefore, a gradual change in $\Lambda_\zeta(y)$ and a sufficiently large k_x were implicitly assumed in the above derivation. However, dropping the second derivative does not change the asymptotic spectrum markedly, compared with the numerical diagonalization of Eq. (20) given in §4.2, but strongly affect the dispersion curves at approximately $k_x = 0$, which is excluded from Eq. (26).

Although the two spectra are connected at $k_x = 0$, they should be regarded as two different modes for the following reasons. First, the second derivative of $\mathcal{E}$ with respect to k_x is discontinuous at $k_x = 0$, although we do not assume any abrupt interface in the above argument. Second, the two field profiles are completely different. One solution has solely the upper component, but the other has solely the lower component. Third, the approximation employed excludes the region at approximately $k_x = 0$. Thus, there should be two domain-wall states having different spectra. The presence of the two modes is consistent with the bulk-edge correspondence, because $|C_+ - C_-| = |\mathrm{sgn}(\Lambda_+) - \mathrm{sgn}(\Lambda_-)| = 2$.

It is remarkable that the two spectra coincide with the asymptotic form of the bulk band edges. We should note that a similar property is obtained for the domain-wall state of the Dirac Hamiltonian:

$$\mathcal{H} = v(k_x\sigma_1 + k_y\sigma_2) + M\sigma_3. \tag{27}$$

The energy spectrum in the bulk is given by $\mathcal{E} = \sqrt{v^2|\boldsymbol{k}|^2 + M^2}$. On the other hand, the domain-wall state for two domains with Dirac masses M of opposite signs has the dispersion relation $\mathcal{E} = vk_x$, irrespective of the domain-wall profile $M(y)$. Again, the dispersion curve of the domain-wall state is the same as the asymptotic behavior of the bulk band edge.

4. Numerical Results and Discussions

To verify the effective Hamiltonian and domain-wall states discussed in the previous sections, we consider a PhC composed of a periodic array of magneto-optical cylinders. The cylindrical axis is taken to be parallel to the z-axis. To make a domain wall, we apply a static antiparallel magnetic field on it, resulting in two domains of the PhC having magneto-optical couplings of the cylinders of opposite signs.

Depending on the lattice structure, the PhC can have C_{3v} (honeycomb lattice composed of two different types of cylinders), C_{4v} (square lattice), and C_{6v} (triangular, honeycomb, and kagome lattices with identical cylinders) point groups if the external magnetic field is zero. All of these groups allow for a double degeneracy at the Γ point. The band gap can be introduced by applying a magnetic field through the magneto-optical effect.

As shown in Appendix A2, such a system can be described by the effective Hamiltonian Eq. (1). In this system gap parameters Λ_ζ of the two domains have opposite signs, because Λ_ζ is proportional to the magneto-optical coupling. A domain wall for photons that is described by Eq. (20) is thus formed in the PhC.

4.1 Bulk

Hereafter, we will focus on a honeycomb lattice PhC with the C_{3v} point group. The PhC is supposed to have isolated quadratic degeneracy at the Γ point under a vanishing external magnetic field. Such a band structure is obtained in the transverse-magnetic (TM) polarization with an asymmetry between the A and B sites. The photonic band structure is obtained by solving the Maxwell equation for the TM polarization:

$$-\boldsymbol{\nabla}\cdot[\xi(\boldsymbol{x})\boldsymbol{\nabla}E_z(\boldsymbol{x})] - \mathrm{i}\{\boldsymbol{\nabla}\times[\zeta(\boldsymbol{x})\boldsymbol{\nabla}E_z(\boldsymbol{x})]\}_z = \frac{\omega^2}{c^2}\epsilon_z(\boldsymbol{x})E_z(\boldsymbol{x}), \tag{28}$$

where ξ and $\mathrm{i}\zeta$ are the diagonal and off-diagonal parts of the inverse permeability, respectively,

$$\begin{pmatrix} \mu_{xx} & \mu_{xy} \\ \mu_{yx} & \mu_{yy} \end{pmatrix}^{-1} = \begin{pmatrix} \xi & \mathrm{i}\zeta \\ -\mathrm{i}\zeta & \xi \end{pmatrix}, \tag{29}$$

and ϵ_z is the z-component of the permittivity. They are periodic in accordance with the honeycomb lattice. We employ the plane-wave expansion method in the actual calculation of the photonic band structure.[17,18]

The photonic band structure without the magneto-optical coupling ζ is shown in Fig. 1. We can find a frequency-isolated Γ point of double degeneracy between the third and fourth bands. We also find a doubly degenerate Γ point between the fifth and sixth bands. However, the latter point overlaps in frequency with other $\boldsymbol{k}$ points in the first BZ. These degeneracies are lifted by the magneto-optical coupling.

Figure 2 shows a close-up view of the third and fourth bands before and after introducing the magneto-optical coupling of the cylinders. The lift is well-described by the parameters of the effective Hamiltonian listed in Table I with

$$\Lambda_\zeta = \lambda^A_\zeta\zeta_A + \lambda^B_\zeta\zeta_B, \tag{30}$$

$$\Lambda_{k\zeta} = \lambda^A_{k\zeta}\zeta_A + \lambda^B_{k\zeta}\zeta_B. \tag{31}$$

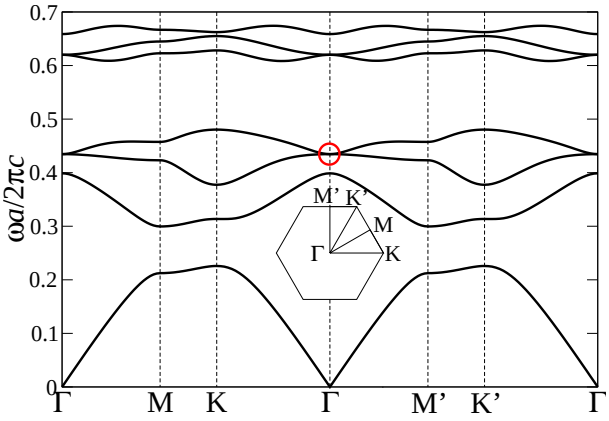

Fig. 1. (Color online) Photonic band structure of the honeycomb-lattice photonic crystal composed of circular cylinders. In the A sites of the honeycomb lattice, the permittivity, (scalar) permeability, and radius of the cylinders are given by $\epsilon_A = 14$, $\mu_A = 1$, and $r_A = 0.25a$, respectively, where a is the lattice constant. Those of the B site are $\epsilon_B = 10$, $\mu_B = 1$, and $r_B = 0.15a$. At the Γ point, an isolated frequency point of quadratic degeneracy is found between the third and fourth bands.

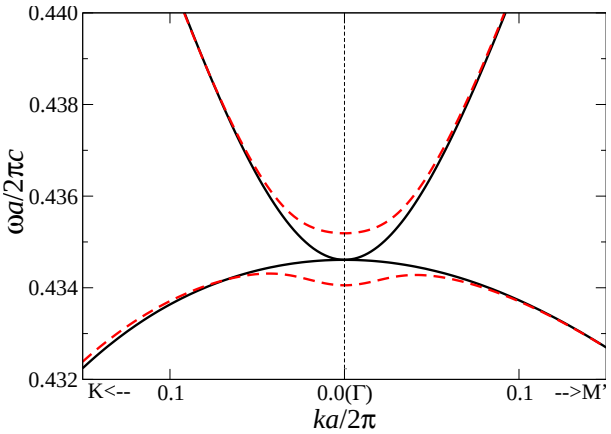

Fig. 2. (Color online) Close-up view of the quadratic degeneracy point indicated by the circle in Fig. 1, before (black sold line) and after (red dashed line) the perturbation of the magneto-optical coupling. The coupling is given by the off-diagonal component of the permeability tensor of the A and B cylinders ($\mu_{xy} = -\mu_{yx} = 0.01\mathrm{i}$). The diagonal components of the permeability tensor are maintained at unity.

These parameters are obtained through Eqs. (12-16) and (A·28-A·32), using the doubly degenerate eigenstate of the unperturbed system.

Numerical calculation of the Chern number C_n of the n-th Bloch band, which is defined by the BZ integral of the Berry curvature[19]

$$C_n = \int_{\mathrm{BZ}} \mathrm{d}^2k(\boldsymbol{\nabla}\times\boldsymbol{A}_{n\boldsymbol{k}})_z, \tag{32}$$

$$\boldsymbol{A}_{n\boldsymbol{k}} = \mathrm{i}\int_{\mathrm{UC}} \mathrm{d}^2x u^*_{n\boldsymbol{k}}(\boldsymbol{x})\epsilon_z(\boldsymbol{x})\boldsymbol{\nabla}_{\boldsymbol{k}}u_{n\boldsymbol{k}}(\boldsymbol{x}), \tag{33}$$

results in $C_3 = 1$ and $C_4 = -1$. Here, $u_{n\boldsymbol{k}}$ is the envelop function of the z-component of the electric field in the n-th Bloch state with the momentum $\boldsymbol{k}$:

$$E_z(\boldsymbol{x}) = u_{n\boldsymbol{k}}(\boldsymbol{x})\mathrm{e}^{\mathrm{i}\boldsymbol{k}\cdot\boldsymbol{x}}, \tag{34}$$

which is solved using the Maxwell equation Eq. (28) in a first-

Table I. Parameters of the effective quadratic Hamiltonian around the doubly degenerate point marked in Fig. 1.

λ_1	λ_2	λ_ζ^A	λ_ζ^B	$\lambda_{k\zeta}^A$	$\lambda_{k\zeta}^B$
0.305	0.384	$-0.0479\times(2\pi/a)^2$	$-0.00145\times(2\pi/a)^2$	$0.00432\times(2\pi/a)$	$-0.0205\times(2\pi/a)$

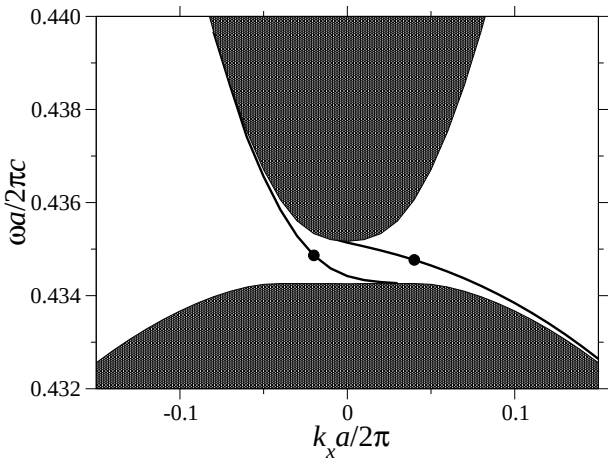

Fig. 3. Dispersion relation of the domain-wall states found numerically in terms of the effective Hamiltonian. The parameters of the effective Hamiltonian are taken from those in Table I. The gap parameter Λ_ζ and the anisotropy parameter $\Lambda_{k\zeta}$ are given in Eqs. (35) and (36), respectively, with $\zeta_A = \zeta_B = -0.01$ and $W = 0.5a$. The shaded region is the projection of the eigenvalues of $\mathcal{H} + \Delta\mathcal{H}$ given in Eqs. (1) and (3). The angular frequency ω is obtained using $\omega = \sqrt{\omega_0^2 + c^2\mathcal{E}}$, where $\omega_0 a/2\pi c = 0.4346$ is the eigenfrequency of the doubly degenerate mode concerned.

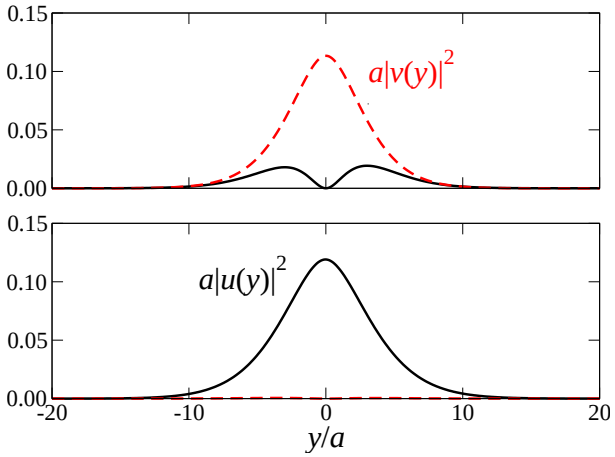

Fig. 4. (Color online) Field profiles of the domain-wall states at $k_x a/2\pi = 0.04$ (upper panel) and -0.02 (lower panel) that are marked in Fig. 3. The normalization of the field is taken to be $\int_{-\infty}^{\infty} dy(|u(y)|^2 + |v(y)|^2) = 1$. The center of the domain wall is at $y = 0$. The black solid and red dashed lines stand for $u(y)$ and $v(y)$, respectively.

principles manner. The Chern numbers are in agreement with those obtained using the effective theory: $C = -\mathrm{sgn}(\Lambda_\zeta) = -1$ for the upper band and $C = \mathrm{sgn}(\Lambda_\zeta) = 1$ for the lower band.

4.2 Domain-wall states in terms of effective theory

Next, we consider the domain-wall states in terms of the effective Hamiltonian. Since the analytical results given in §3 are obtained by rough approximation, we present here a numerical solution of the domain-wall states. Figure 3 shows the dispersion relation of the domain-wall states derived by discretizing Eq. (21), taking account of the additional term Eq. (3). As the gap function $\Lambda_\zeta(y)$, we assume the following forms:

$$\Lambda_\zeta(y) = \Lambda_+ \tanh\left(\frac{y}{W}\right), \tag{35}$$

$$\Lambda_{k\zeta}(y) = \Lambda_{k\zeta+} \tanh\left(\frac{y}{W}\right), \tag{36}$$

$$\Lambda_+ = \lambda_\zeta^A \zeta_A + \lambda_\zeta^B \zeta_B, \tag{37}$$

$$\Lambda_{k\zeta+} = \lambda_{k\zeta}^A \zeta_A + \lambda_{k\zeta}^B \zeta_B, \tag{38}$$

where the center of the domain wall is taken to be $y = 0$ and W is the domain-wall width. As predicted in §3, we obtain two dispersion curves that terminate at different bands. One curve lies almost at a positive $k_\parallel$, while the other is at a negative $k_\parallel$. The slopes of the two curves are different, but are both negative. In addition, their asymptotic spectra coincide with the bulk band edges. These features indicate that the two curves are certainly chiral and those predicted with a rough approximation in §3. Although not shown, we can find that the spectra do not change markedly with decreasing domain-wall width W. Thus, the domain-wall states have, to some extent, a topological nature as in the domain-wall state of the Dirac Hamiltonian.

The field profiles of the domain-wall states at the marked points in Fig. 3 are shown in Fig. 4. In our case, both λ_1 and λ_2 are positive and satisfy $\lambda_1 < \lambda_2$. The results in §3 indicate that the mode of positive k_x has a vanishing u, the upper component of a "pseudo-spin". In agreement with this statement, the mode has a rather dominant v, the lower component of the pseudo-spin. Similarly, the mode of negative k_x has u as the dominant component. The localization length exhibits reasonable agreement with rough estimate of $L = |2\lambda_2 k_x/\Lambda_+| \simeq 4.95a$ at $k_x a/2\pi = -0.02$.

4.3 Domain wall in terms of first-principles calculation

Finally, we consider the domain-wall states of photons in a first-principles calculation. The possible domain-wall states in the PhC under study can be evaluated using the 2d version of the photonic Korringa-Kohn-Rostoker method.[20] Suppose that the two domains have an infinite width parallel to the domain wall, but a finite thickness perpendicular to the domain wall. The scattering (S) matrix is then defined for the finite-thickness PhC. By energy conservation, the S-matrix is shown to be unitarized. The S-matrix allows us to evaluate the optical density of states (DOS) ρ in the finite-thickness PhC via the scattering phase shift δ:

$$\rho = \frac{1}{\pi}\frac{\partial\delta}{\partial\omega}. \tag{39}$$

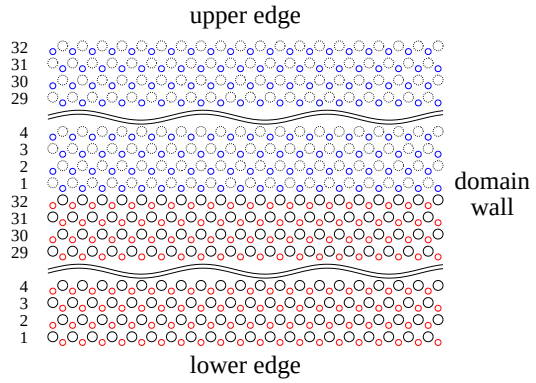

Fig. 5. (Color online) Schematic illustration of the system under study. It consists of two domains of a honeycomb-lattice photonic crystal. In one domain, the magneto-optical coupling is positive, while in the other domain it is positive. The domain wall and edges are of the zigzag type of the honeycomb lattice.

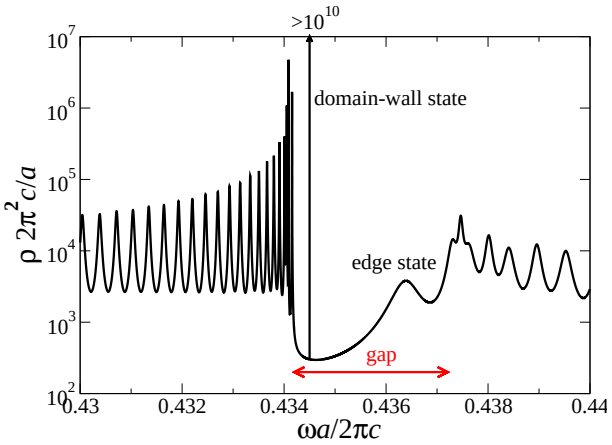

Fig. 6. (Color online) Optical density of states ρ in 32+32-layer-thick photonic crystal having the two domains. The momentum $k_\parallel$ parallel to the domain wall as well as the lower and upper edges is taken to be $0.06\times 2\pi/a$. Two domains are characterized by magneto-optical couplings of the cylinders of opposite signs: $\kappa_A = \kappa_B = -0.01$ (lower domain) and $\kappa_A = \kappa_B = 0.01$ (upper domain). Each domain has a 32 layer thickness and zigzag edges, as shown in Fig. 5.

Here, the phase shift is obtained via the determinant of the unitarized S-matrix $\tilde{S}$:

$$\delta = \frac{1}{2i}\log\det\tilde{S}, \quad \tilde{S}^\dagger\tilde{S} = 1. \tag{40}$$

We refer to Ref. 21 for the explicit construction of the unitarized S-matrix.

A domain-wall state is identified as a sharp Lorentzian peak of the optical density of states at a fixed parallel momentum $k_\parallel$. The peak is found in the pseudo-gap of the bulk photonic band structure of the two domains. The peak becomes sharper with increasing layer thickness of the two domains. We should note that this method also allows us to identify edge states localized at either the lower or upper edge.[22] In contrast to the domain-wall states, the edge states are insensitive to the thickness of the two domains.

By setting the two domains with magneto-optical couplings of opposite signs, we consider the domain-wall states of photons in the honeycomb lattice PhC. The geometry assumed in the numerical calculation is shown in Fig. 5.

Figure 6 shows the optical DOS in the finite-thickness PhC at a fixed $k_\parallel$. The DOS spectrum exhibits a sequence of peaks in the bulk band region as well as an sharp and broad isolated peaks in the gap region. The former peak in the gap is a domain-wall state, while the latter peak is an edge state.

By scanning $k_\parallel$, we can obtain the photonic band structure of the domain-wall states and edge states. The numerical results of the first-principles calculation are shown in Fig. 7 for a zigzag geometry of the domain wall and edges. Several dispersion curves are found in the gap region. Among them, two curves (shown by solid line) are almost the same as those in Fig. 3. Therefore, the agreement between the results of the first-principles calculation and effective-theory calculation is fairly good. The other curves shown by dashed and dash-dotted lines are of the upper and lower edge states, respectively. We should note that the two dash-dotted curves are connected at the boundary of the surface BZ ($k_x a/2\pi = \pm 0.5$). Therefore, there is only one curve per edge that terminates at different bulk bands. Thus, these curves of the edge states have the same chirality, but their chirality is opposite to that of

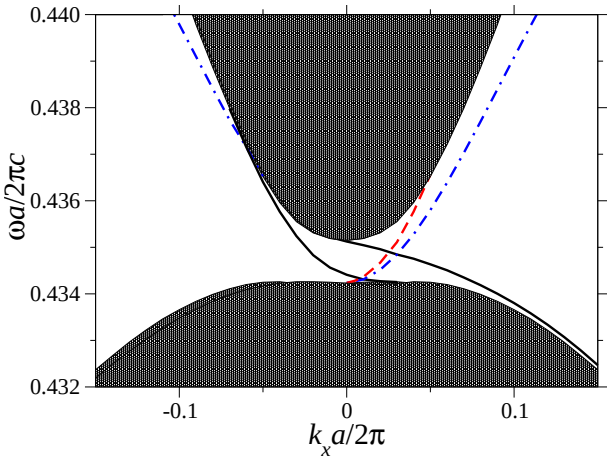

Fig. 7. (Color online) Photonic band structure of the domain-wall states (black solid line) and edge states (dashed and dash-dotted lines) in terms of the photonic Korringa-Kohn-Rostoker method. The red dashed and blue dash-dotted lines indicate the upper and lower edge states, respectively. The shaded region is the projection of the bulk band structures of the two domains.

the domain-wall states. This property is fully consistent with the bulk-edge correspondence.

Concerning the armchair geometry of the domain wall, we can find nearly the same dispersion curves of the domain-wall states (not shown) as in the zigzag geometry. This property can be drawn from the rather small anisotropy of the effective Hamiltonian as well as the topological nature of the domain-wall states. The upper and the lower edge states are shown to be degenerate owing to the mirror symmetry with respect to the domain wall[22] (note that the mirror reflection inverts the applied magnetic field). The resulting band structure of the edge states is similar to that of the lower edge state (indicated by dash-dotted line in Fig. 7).

5. Conclusion

We have derived, with the aid of the group theory, an effective quadratic Hamiltonian for a doubly degenerate mode at the BZ center in an unperturbed system. Its eigenstates can have a nontrivial topology with the Chern number of ± 1 if a TRS-breaking perturbation is introduced. We have found that two domain-wall states with the same chirality can emerge at the interface between two domains whose low-energy excitation is described by the quadratic Hamiltonian. To obtain such domain-wall states, the gap parameters Λ_ζ of the two domains must have opposite signs. The two domain-wall states have dispersion curves that coincide asymptotically to the band edges of the projected band structure in the bulk.

Furthermore, we have presented an explicit example, the honeycomb-lattice PhC, that is described by such an effective Hamiltonian for photons. By a first-principles calculation of photonic eigenstates, we have shown that two domain-wall states with the same chirality emerge at the interface between two domains with opposite magneto-optical couplings. A good agreement is obtained between the results of first-principles calculation and calculation based on the effective Hamiltonian.

Quite recently, similar domain-wall states with chirality have been predicted in bilayer graphene.[23] By applying an interlayer electric field, a gap opens in the two valleys of K and K' (see the inset of Fig. 1 for the notation) around the BZ corner. There, a quadratic dispersion similar to ours emerges, having the Berry phase of 2π[24] in each valley. As a result, the domain wall formed by AB and BA Bernal stacking regions has two domain-wall states *per valley* with the same chirality. Since the TRS is preserved in such a system, the Chern numbers of the relevant bands are zero. As a result, the chiralities of the domain-wall states are opposite between the K and K' valleys. In contrast, our domain-wall states originate from the gapped quadratic dispersion around the BZ center. A TRS-breaking perturbation is crucial in our case, resulting in a nonzero Chern number.

Acknowledgment

This work was partially supported by KAKENHI (Grant No. 23540380) of the Japan Society for the Promotion of Science.

Appendix A: Two Physical Systems Having Effective Quadratic Hamiltonians

In this appendix we provide further details on the effective Hamiltonian and derive its symmetry constraints Eqs. (5-9) for two kinds of physical systems.

A.1 Electron under periodic potential and periodic magnetic field

We first consider an electron under a periodic potential and a periodic magnetic field. Its original Hamiltonian is given by Eqs. (10) and (11). Let us start with the plane-wave expansion form of the Schrödinger equation. Using the Bloch theorem, the wave function of Bloch momentum $\boldsymbol{k}$ is written as

$$\psi(\boldsymbol{x}) = \sum_{\boldsymbol{g}} \mathrm{e}^{\mathrm{i}(\boldsymbol{k}+\boldsymbol{g})\cdot\boldsymbol{x}} u_{\boldsymbol{g}}, \tag{A·1}$$

where $\boldsymbol{g}$ is a 2d reciprocal lattice vector. Similarly, the scalar

panded as

$$\begin{aligned} V(\boldsymbol{x}) &= \sum_{\boldsymbol{g}} \mathrm{e}^{\mathrm{i}\boldsymbol{g}\cdot\boldsymbol{x}} V_{\boldsymbol{g}}, \\ \boldsymbol{A}(\boldsymbol{x}) &= \sum_{\boldsymbol{g}} \mathrm{e}^{\mathrm{i}\boldsymbol{g}\cdot\boldsymbol{x}} \boldsymbol{A}_{\boldsymbol{g}}, \\ B_z(\boldsymbol{x}) &= \sum_{\boldsymbol{g}} \mathrm{e}^{\mathrm{i}\boldsymbol{g}\cdot\boldsymbol{x}} B_{\boldsymbol{g}}. \end{aligned} \tag{A·2}$$

Since, by definition, $(\boldsymbol{\nabla}\times\boldsymbol{A})_z = B_z$, the Fourier component $\boldsymbol{A}_{\boldsymbol{g}}$ of the vector potential is written as

$$\boldsymbol{A}_{\boldsymbol{g}} = \mathrm{i}\left(\frac{g_y}{|\boldsymbol{g}|^2}, -\frac{g_x}{|\boldsymbol{g}|^2}\right) B_{\boldsymbol{g}}. \tag{A·3}$$

We should note that the singularity at $\boldsymbol{g} = \boldsymbol{0}$ is absent, because we assume a vanishing magnetic flux per UC, namely, $B_{\boldsymbol{g}=\boldsymbol{0}} = 0$. The Schrödinger equation now becomes

$$\sum_{\boldsymbol{g}'} \left[(H_0)_{\boldsymbol{g}\boldsymbol{g}'} + (H')_{\boldsymbol{g}\boldsymbol{g}'}\right] u_{\boldsymbol{g}'} = E u_{\boldsymbol{g}}, \tag{A·4}$$

$$(H_0)_{\boldsymbol{g}\boldsymbol{g}'} = \frac{(\hbar\boldsymbol{g})^2}{2m}\delta_{\boldsymbol{g}\boldsymbol{g}'} + V_{\boldsymbol{g}-\boldsymbol{g}'}, \tag{A·5}$$

$$(H')_{\boldsymbol{g}\boldsymbol{g}'} = \frac{1}{2m}\left[\hbar^2(\boldsymbol{k}^2 + 2\boldsymbol{k}\cdot\boldsymbol{g})\delta_{\boldsymbol{g}\boldsymbol{g}'} + \hbar e(2\boldsymbol{k} + \boldsymbol{g} + \boldsymbol{g}')\cdot\boldsymbol{A}_{\boldsymbol{g}-\boldsymbol{g}'} + e^2\sum_{\boldsymbol{g}''}\boldsymbol{A}_{\boldsymbol{g}-\boldsymbol{g}''}\cdot\boldsymbol{A}_{\boldsymbol{g}''-\boldsymbol{g}'}\right], \tag{A·6}$$

where H_0 and H' are the unperturbed and perturbed parts of the original Hamiltonian, respectively.

As described in this paper, we assume the point group symmetry $\mathcal{G}$ that allows for a doubly degenerate representation in the unperturbed system. Suppose that A is an element of $\mathcal{G}$. Then, we have $V(A\boldsymbol{x}) = V(\boldsymbol{x})$ for the scalar potential. In terms of the Fourier component, we have $V_{A\boldsymbol{g}} = V_{\boldsymbol{g}}$ for an arbitrary $\boldsymbol{g}$. As a result, the unperturbed eigenmode $u_{\boldsymbol{g}}^{(0p)}$ $(p = 1, 2)$ of a doubly degenerate representation R of $\mathcal{G}$ satisfies

$$\sum_{\boldsymbol{g}'}(H_0)_{\boldsymbol{g}\boldsymbol{g}'} u_{\boldsymbol{g}'}^{(0p)} = E_0^{(0)} u_{\boldsymbol{g}}^{(0p)}, \tag{A·7}$$

$$u^{(0p)}_{A^{-1}\boldsymbol{g}} = \sum_{q=1,2} u^{(0q)}_{\boldsymbol{g}} [D_R(A)]_{qp}, \tag{A·8}$$

where $D_R(A)$ is a 2×2 unitary representation matrix of A. Similarly, modes denoted by (n) other than the degenerate mode concerned are classified according to the IRRs of $\mathcal{G}$. Thus, we have

$$\sum_{\boldsymbol{g}'} (H_0)_{\boldsymbol{g}\boldsymbol{g}'} u^{(n)}_{\boldsymbol{g}'} = E^{(n)}_0 u^{(n)}_{\boldsymbol{g}}, \tag{A·9}$$

$$u^{(n)}_{A^{-1}\boldsymbol{g}} = \sum_{n'=1}^{\dim R'} u^{(n')}_{\boldsymbol{g}} [D_{R'}(A)]_{n'n}, \tag{A·10}$$

where R' stands for the IRR to which the state (n) belongs. The effective Hamiltonian for the degenerate mode under the $\boldsymbol{k}\cdot\boldsymbol{p}$ perturbation and the perturbation of the periodic magnetic field is given by Eq. (4).

For simplicity, from now on we will assume that the periodic magnetic field itself obeys all the spatial symmetries of the periodic potential. Thus, we have $B_z(A\boldsymbol{x}) = B_z(\boldsymbol{x})$, namely, $B_{A\boldsymbol{g}} = B_{\boldsymbol{g}}$. We should note that this property does not imply the conservation of all the spatial symmetries of the unperturbed system. Actually, the parity and TRS are broken by the magnetic field because of the axial-vector nature of the magnetic field. In the simplest case, the periodic magnetic field is given by the reciprocal-lattice components of the nearest-neighbor (NN) sites from the origin as

$$B_{\boldsymbol{g}} = \begin{cases} \zeta & \text{for } \boldsymbol{g} \in NN \\ 0 & \text{otherwise} \end{cases}. \tag{A·11}$$

In this case the degree of TRS breaking due to the periodic magnetic field is parametrized by ζ.

In the effective Hamiltonian, the terms up to the second order in $\boldsymbol{k}$ and ζ are given by

$$[\mathcal{H}^{(k)}]_{pq} = \sum_{\boldsymbol{g}} (u^{(0p)}_{\boldsymbol{g}})^* \frac{\hbar^2}{m} \boldsymbol{k}\cdot\boldsymbol{g} u^{(0q)}_{\boldsymbol{g}}, \tag{A·12}$$

$$[\mathcal{H}^{(\zeta)}]_{pq} = \sum_{\boldsymbol{g}\boldsymbol{g}'} (u^{(0p)}_{\boldsymbol{g}})^* \frac{\mathrm{i}\hbar e}{2m} \frac{[(\boldsymbol{g}+\boldsymbol{g}')\times(\boldsymbol{g}-\boldsymbol{g}')]_z}{|\boldsymbol{g}-\boldsymbol{g}'|^2} B_{\boldsymbol{g}-\boldsymbol{g}'} u^{(0q)}_{\boldsymbol{g}'}, \tag{A·13}$$

$$[\mathcal{H}^{(k^2)}]_{pq} = \frac{(\hbar\boldsymbol{k})^2}{2m}\delta_{pq} + \sum_{n\neq 0} \frac{[\mathcal{H}^{(k)}]_{pn}[\mathcal{H}^{(k)}]_{nq}}{E^{(0)}_0 - E^{(n)}_0}, \tag{A·14}$$

$$[\mathcal{H}^{(\zeta^2)}]_{pq} = -\sum_{\boldsymbol{g}\boldsymbol{g}'\boldsymbol{g}''} (u^{(0p)}_{\boldsymbol{g}})^* \frac{e^2}{2m} \frac{(\boldsymbol{g}-\boldsymbol{g}'')\cdot(\boldsymbol{g}''-\boldsymbol{g}')}{|\boldsymbol{g}-\boldsymbol{g}''|^2|\boldsymbol{g}''-\boldsymbol{g}'|^2} B_{\boldsymbol{g}-\boldsymbol{g}''} B_{\boldsymbol{g}''-\boldsymbol{g}'} u^{(0q)}_{\boldsymbol{g}'} + \sum_{n\neq 0} \frac{[\mathcal{H}^{(\zeta)}]_{pn}[\mathcal{H}^{(\zeta)}]_{nq}}{E^{(0)}_0 - E^{(n)}_0}, \tag{A·15}$$

$$[\mathcal{H}^{(k\zeta)}]_{pq} = \sum_{\boldsymbol{g}\boldsymbol{g}'} (u^{(0p)}_{\boldsymbol{g}})^* \frac{\mathrm{i}\hbar e}{2m} \frac{[\boldsymbol{k}\times(\boldsymbol{g}-\boldsymbol{g}')]_z}{|\boldsymbol{g}-\boldsymbol{g}'|^2} B_{\boldsymbol{g}-\boldsymbol{g}'} u^{(0q)}_{\boldsymbol{g}'} + \sum_{n\neq 0} \frac{[\mathcal{H}^{(k)}]_{pn}[\mathcal{H}^{(\zeta)}]_{nq} + [\mathcal{H}^{(\zeta)}]_{pn}[\mathcal{H}^{(k)}]_{nq}}{E^{(0)}_0 - E^{(n)}_0}. \tag{A·16}$$

By using Eq. (A·8), we readily obtain the symmetry constraint of the first-order terms, namely, Eqs. (5) and (7). The second-order terms involve the matrix elements relevant to the intermediate states. Such matrix elements also satisfy similar relations to Eqs. (5) and (7):

$$[\mathcal{H}^{(k)}(\boldsymbol{k})]_{pn} = \sum_{p'n'} [D^\dagger_R(A)]_{pp'} [\mathcal{H}^{(k)}(A\boldsymbol{k})]_{p'n'} [D_{R'}(A)]_{n'n}, \tag{A·17}$$

$$[\mathcal{H}^{(\zeta)}]_{pn} = \det A^{-1} \sum_{p'n'} [D^\dagger_R(A)]_{pp'} [\mathcal{H}^{(\zeta)}]_{p'n'} [D_{R'}(A)]_{n'n}. \tag{A·18}$$

With the aid of the unitarity of the representation matrix $D_{R'}(A)$, namely, $D_{R'}(A)D^\dagger_{R'}(A) = 1$, we can obtain Eqs. (6), (8), and (9).

A.2 Photon in photonic crystal with magneto-optical effect

Next, we consider photons (strictly speaking, classical light wave) in a PhC composed of a 2d periodic array of circular cylinders with the magneto-optical effect. A static external magnetic field is applied in the z-direction. We restrict ourselves to the in-plane propagation of light, so that two transverse-polarization degrees of light are decoupled into the so-called transverse electric (TE) and TM.[17] In the TE (TM) polarization only the z-component of the magnetic (electric) field is nonzero.[17] We consider the TM polarization here. The Maxwell equation for the system under consideration is given by Eqs. (28) and (29).

Using the Bloch theorem, the z-component of the electric field with the Bloch momentum $\boldsymbol{k}$ can be expanded as

$$E_z(\boldsymbol{x}) = \sum_{\boldsymbol{g}} \mathrm{e}^{\mathrm{i}(\boldsymbol{k}+\boldsymbol{g})\cdot\boldsymbol{x}} u_{\boldsymbol{g}}. \tag{A·19}$$

Here, we assume the time-harmonic dependence of the angular frequency ω, and thus the actual (real-value and time-dependent) electric field is given by

$$E_z(\boldsymbol{x}, t) = \Re[E_z(\boldsymbol{x})\mathrm{e}^{-\mathrm{i}\omega t}]. \tag{A·20}$$

The permittivity $\epsilon_z(\boldsymbol{x})$ and the inverse permeability, diagonal term $\xi(\boldsymbol{x})$ and off-diagonal term $\pm\mathrm{i}\zeta(\boldsymbol{x})$, in the PhC can be expanded as

$$\theta(\boldsymbol{x}) = \sum_{\boldsymbol{g}} \mathrm{e}^{\mathrm{i}\boldsymbol{g}\cdot\boldsymbol{x}} \theta_{\boldsymbol{g}} \quad (\theta = \epsilon_z, \xi, \zeta). \tag{A·21}$$

The imaginary part in the permeability represents a broken TRS in the Maxwell equation, and thus $\zeta(\boldsymbol{x})$, i.e., the magneto-optical coupling, stands for the degree of TRS breaking. The Maxwell equation is transformed into

$$\sum_{g'}[(H_0)_{gg'} + (H')_{gg'}]u_{g'} = E\sum_{g'}K_{gg'}u_{g'}, \quad E = \frac{\omega^2}{c^2}, \tag{A·22}$$

$$(H_0)_{gg'} = \xi_{g-g'}\boldsymbol{g}\cdot\boldsymbol{g}', \quad K_{gg'} = \epsilon_{zg-g'}, \tag{A·23}$$

$$(H')_{gg'} = \xi_{g-g'}\left[|\boldsymbol{k}|^2 + \boldsymbol{k}\cdot(\boldsymbol{g}+\boldsymbol{g}')\right] + \mathrm{i}\zeta_{g-g'}\left[-\boldsymbol{k}\times(\boldsymbol{g}-\boldsymbol{g}') + \boldsymbol{g}\times\boldsymbol{g}'\right]_z. \tag{A·24}$$

We assume piecewise constant permittivity and permeability. Namely, we have constant θ_a and θ_b values inside and outside the cylinders, respectively, for $\theta = \xi, \zeta$, and ϵ_z. As a result, the Fourier component $\theta_{\boldsymbol{g}}$ is given by

$$\theta_{\boldsymbol{g}} = \theta_b\delta_{\boldsymbol{g}\boldsymbol{0}} + \sum_{a\in\mathrm{UC}}(\theta_a-\theta_b)2f_a\frac{J_1(|\boldsymbol{g}|r_a)}{|\boldsymbol{g}|r_a}\mathrm{e}^{-\mathrm{i}\boldsymbol{g}\cdot\boldsymbol{x}_a}, \tag{A·25}$$

where f_a, r_a, and $\boldsymbol{x}_a$ are the filling ratio, radius, and 2d central coordinate of the cylinder a, respectively, and J_1 is the Bessel function of the first order.

Since we are considering a PhC in which the magneto-optical effect is limited in the cylinders, we put $\zeta_b = 0$. Therefore, the broken TRS is parametrized by ζ_a, the magneto-optical coupling of the cylinders. The magneto-optical coupling is proportional to the spontaneous magnetization through the Larmor precession.[25] It is thus controllable by applying an external magnetic field.

In what follows, we assume the point group symmetry $\mathcal{G}$ in the unperturbed system described by H_0 and K, and consider the perturbation H' that includes the $\boldsymbol{k}\cdot\boldsymbol{p}$ perturbation and the TRS-breaking perturbation due to the magneto-optical coupling ζ_g. Therefore, we have $\theta_{Ag} = \theta_g$ ($A \in \mathcal{G}$) for $\theta = \xi, \zeta$, and ϵ_z. Thus, the eigenmodes of the unperturbed system satisfy

$$\sum_{g'}(H_0)_{gg'}u^{(0p)}_{g'} = E^{(0)}_0\sum_{g'}K_{gg'}u^{(0p)}_{g'}, \tag{A·26}$$

$$\sum_{g'}(H_0)_{gg'}u^{(n)}_{g'} = E^{(n)}_0\sum_{g'}K_{gg'}u^{(n)}_{g'}, \tag{A·27}$$

for a doubly degenerate mode and the other modes, respectively. Starting with the doubly degenerate eigenmode of IRR R, its effective Hamiltonian is given by Eq. (4). In the effective Hamiltonian, the terms up to the second order in $\boldsymbol{k}$ and ζ are given by

$$\mathcal{H}^{(k)}_{pq} = \sum_{gg'}(u^{(0p)}_{g})^*\xi_{g-g'}\boldsymbol{k}\cdot(\boldsymbol{g}+\boldsymbol{g}')u^{(0q)}_{g'}, \tag{A·28}$$

$$\mathcal{H}^{(\zeta)}_{pq} = \sum_{gg'}(u^{(0p)}_{g})^*\mathrm{i}\zeta_{g-g'}(\boldsymbol{g}\times\boldsymbol{g}')_z u^{(0q)}_{g'}, \tag{A·29}$$

$$\mathcal{H}^{(k^2)}_{pq} = |\boldsymbol{k}|^2\sum_{gg'}(u^{(0p)}_{g})^*\xi_{g-g'}u^{(0q)}_{g'} + \sum_{n\neq 0}\frac{[\mathcal{H}^{(k)}]_{pn}[\mathcal{H}^{(k)}]_{nq}}{E^{(0)}_0 - E^{(n)}_0}, \tag{A·30}$$

$$\mathcal{H}^{(\zeta^2)}_{pq} = \sum_{n\neq 0}\frac{[\mathcal{H}^{(\zeta)}]_{pn}[\mathcal{H}^{(\zeta)}]_{nq}}{E^{(0)}_0 - E^{(n)}_0}, \tag{A·31}$$

$$\mathcal{H}^{(k\zeta)}_{pq} = \sum_{gg'}(u^{(0p)}_{g})^*\mathrm{i}\zeta_{g-g'}[\boldsymbol{k}\times(\boldsymbol{g}'-\boldsymbol{g})]_z u^{(0q)}_{g'} + \sum_{n\neq 0}\frac{[\mathcal{H}^{(k)}]_{pn}[\mathcal{H}^{(\zeta)}]_{nq} + [\mathcal{H}^{(\zeta)}]_{pn}[\mathcal{H}^{(k)}]_{nq}}{E^{(0)}_0 - E^{(n)}_0}. \tag{A·32}$$

Since Eqs. (A·8) and (A·10) can also be applied to the doubly degenerate mode and the other modes, respectively, it is not difficult to derive Eqs. (5)-(9).

Appendix B: Quadratic Hamiltonian from Symmetry Constraints

Once we have the symmetry constraints Eqs. (5)-(9), we can neglect the detailed expression of the effective Hamiltonian. The representation theory of the point group $\mathcal{G}$ enables us to derive a possible form of the effective Hamiltonian. Lattice systems having either $\mathcal{G} = C_{6v}$ or C_{4v} or C_{3v} lead to our quadratic effective Hamiltonian. A schematic illustration of the geometry of the lattice systems is shown in Fig. B·1.

B.1 C_{6v}

The C_{6v} point group consists of $\{1, 2C_6, 2C_3, C_2, 3\sigma_y, 3\sigma_x\}$ and allows for two 2d IRRs (E_1 and E_2) and four one-dimensional (1d) IRRs (A_1, A_2, B_1, and B_2).[26] Let us first consider the E_1 mode. Its unitary representation matrices showing modulo unitary equivalence are given by

$$D_{E_1}(C_6) = \begin{pmatrix} \frac{1}{2} & -\frac{\sqrt{3}}{2} \\ \frac{\sqrt{3}}{2} & \frac{1}{2} \end{pmatrix}, \quad D_{E_1}(\sigma_x) = \begin{pmatrix} -1 & 0 \\ 0 & 1 \end{pmatrix},$$
$$D_{E_1}(C_3) = \begin{pmatrix} -\frac{1}{2} & -\frac{\sqrt{3}}{2} \\ \frac{\sqrt{3}}{2} & -\frac{1}{2} \end{pmatrix}, \quad D_{E_1}(\sigma_y) = \begin{pmatrix} 1 & 0 \\ 0 & -1 \end{pmatrix},$$
$$D_{E_1}(C_2) = \begin{pmatrix} -1 & 0 \\ 0 & -1 \end{pmatrix}. \tag{B·1}$$

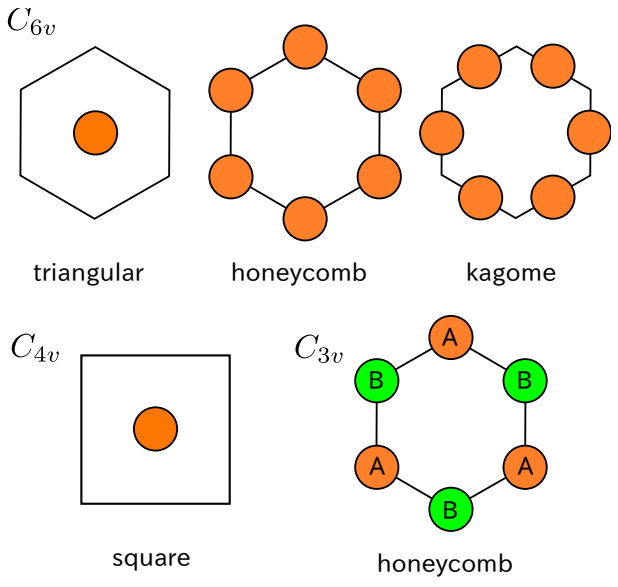

Fig. B·1. (Color online) Geometries of the unit cells in the lattice systems having C_{6v}, C_{4v}, and C_{3v} point groups.

The first-order term in $\boldsymbol{k}$ of the effective Hamiltonian is generally written as

$$\mathcal{H}^{(k)} = k_x C_x + k_y C_y, \tag{B·2}$$

where $C_{x(y)}$ is a 2×2 hermite matrix. By applying $A = C_2$, namely, π rotation in Eq. (5), we immediately have $C_x = C_y = 0$. Therefore, $\mathcal{H}^{(k)} = 0$ is obtained. The second-order term in $\boldsymbol{k}$ is written as

$$\mathcal{H}^{(k^2)} = k_x^2 C_{xx} + k_y^2 C_{yy} + k_x k_y C_{xy}, \tag{B·3}$$

with the 2×2 hermite matrices C_{xx}, C_{yy}, and C_{xy}. Although a possible form of $\mathcal{H}^{(k^2)}$ is determined by applying various $A(\in C_{6v})$ in Eq. (6), it is more convenient to consider the matrix elements relevant to the intermediate states. To this end, we list up the representation matrices of the other IRRs of C_{6v}. Those of the E_2 representation are given by

$$D_{E_2}(C_6) = \begin{pmatrix} -\frac{1}{2} & \frac{\sqrt{3}}{2} \\ -\frac{\sqrt{3}}{2} & -\frac{1}{2} \end{pmatrix}, \quad D_{E_2}(\sigma_x) = \begin{pmatrix} -1 & 0 \\ 0 & 1 \end{pmatrix},$$
$$D_{E_2}(C_3) = \begin{pmatrix} -\frac{1}{2} & -\frac{\sqrt{3}}{2} \\ \frac{\sqrt{3}}{2} & -\frac{1}{2} \end{pmatrix}, \quad D_{E_2}(\sigma_y) = \begin{pmatrix} -1 & 0 \\ 0 & 1 \end{pmatrix},$$
$$D_{E_2}(C_2) = \begin{pmatrix} 1 & 0 \\ 0 & 1 \end{pmatrix}. \tag{B·4}$$

As for the 1d representations, the character table of C_{6v} gives the following:[26]

$$D_{A_1}(A) = 1 \ (\forall A \in C_{6v}), \tag{B·5}$$

$$D_{A_2}(A) = \begin{cases} 1 & \text{for } A = C_6, C_3, C_2 \\ -1 & \text{for } A = \sigma_x, \sigma_y \end{cases}, \tag{B·6}$$

$$D_{B_1}(A) = \begin{cases} 1 & \text{for } A = C_3, \sigma_y \\ -1 & \text{for } A = C_6, C_2, \sigma_x \end{cases}, \tag{B·7}$$

$$D_{B_2}(A) = \begin{cases} 1 & \text{for } A = C_3, \sigma_x \\ -1 & \text{for } A = C_6, C_2, \sigma_y \end{cases}. \tag{B·8}$$

By applying Eq. (A·17) for various representations of the intermediate states (n), we find

$$\mathcal{H}^{(k)}_{E_1A_1} \propto \begin{pmatrix} k_x \\ k_y \end{pmatrix}, \quad \mathcal{H}^{(k)}_{E_1A_2} \propto \begin{pmatrix} -k_y \\ k_x \end{pmatrix},$$
$$\mathcal{H}^{(k)}_{E_1B_1} = \mathcal{H}^{(k)}_{E_1B_2} = 0,$$
$$\mathcal{H}^{(k)}_{E_1E_1} = 0, \quad \mathcal{H}^{(k)}_{E_1E_2} \propto \begin{pmatrix} k_y & k_x \\ k_x & -k_y \end{pmatrix}. \tag{B·9}$$

The other matrix elements, such as $\mathcal{H}^{(k)}_{A_1E_1}$, are simply given by the hermite conjugation $\mathcal{H}^{(k)}_{A_1E_1} = (\mathcal{H}^{(k)}_{E_1A_1})^\dagger$. Summing up all the intermediate states in Eq. (A·14) or (A·30), classified by the IRRs of C_{6v}, we have

$$\mathcal{H}^{(k^2)} = (c_0 + c_{E_2})|\boldsymbol{k}|^2 \hat{1} + c_{A_1} \begin{pmatrix} k_x^2 & k_x k_y \\ k_x k_y & k_y^2 \end{pmatrix} + c_{A_2} \begin{pmatrix} k_y^2 & -k_x k_y \\ -k_x k_y & k_x^2 \end{pmatrix}, \tag{B·10}$$

where c_0 is the contribution of the direct term that does not involve the intermediate states, and $c_{R'}$ ($R' = A_1, A_2, E_2$) is the contributions of the intermediates states with IRR R'. The above expression is cast into Eq. (13).

As for the first-order term in ζ, we first apply $A = \sigma_x$ (parity transformation with respect to x) to Eq. (7). It immediately leads to the vanishment of the diagonal elements of $\mathcal{H}^{(\zeta)}$. Then, by applying $A = C_6$ ($\pi/3$ rotation), we find $\mathcal{H}^{(\zeta)} = \Lambda_\zeta \sigma_2$. By definition, the parameter Λ_ζ depends linearly on $B_{\boldsymbol{g}}$ for electrons and on $\zeta_{\boldsymbol{g}}$ for photons. In the former case, we assume Eq. (A·11). Therefore, Λ is proportional to ζ, the Fourier component of the periodic magnetic field. In the latter case, we assume Eq. (A·25). Therefore, Λ_ζ is linear in ζ_a, the magneto-optical coupling of the cylinders, which is proportional to the spontaneous magnetization. Thus, the gap parameter Λ_ζ of our quadratic Hamiltonian Eq. (1) is controllable by an external magnetic field in both systems.

The second-order term in ζ satisfies Eq. (8). By applying $A = \sigma_x$, the off-diagonal terms of $\mathcal{H}^{(\zeta^2)}$ vanish. Furthermore, putting $A = C_6$ results in $\mathcal{H}^{(\zeta^2)} \propto \hat{1}$. The other A's do not restrict the above form. Therefore, this term only shifts the eigenvalues, and can therefore be neglected. We also note that this form is consistent with the contribution of the sum over the intermediate states. Actually, by solving Eq. (A·18), we obtain

$$\mathcal{H}^{(\zeta)}_{E_1A_1} = \mathcal{H}^{(\zeta)}_{E_1A_2} = \mathcal{H}^{(\zeta)}_{E_1B_1} = \mathcal{H}^{(\zeta)}_{E_1B_2} = 0,$$
$$\mathcal{H}^{(\zeta)}_{E_1E_1} \propto \begin{pmatrix} 0 & 1 \\ -1 & 0 \end{pmatrix}, \quad \mathcal{H}^{(\zeta)}_{E_1E_2} = 0. \tag{B·11}$$

Summing up all the intermediate states, we again obtain a constant shift.

Finally, the cross term between $\boldsymbol{k}$ and ζ is generally written as

$$\mathcal{H}^{(k\zeta)} = k_x D_x + k_y D_y, \tag{B·12}$$

where $D_{x(y)}$ is a 2×2 matrix. By applying $A = C_2$ in Eq. (9), we obtain $D_x = D_y = 0$ and thus $\mathcal{H}^{(k\zeta)} = 0$, as in the case of the first-order term in $\boldsymbol{k}$. This result is again consistent with the sum over the intermediate states. In summary, we obtain Eq. (1) for an E_1 degenerate mode.

A similar argument is available for an E_2 degenerate mode. The resulting form of the effective Hamiltonian is nothing but

Eq. (1). The matrix elements relevant for showing the result are summarized as follows:

$$\mathcal{H}^{(k)}_{E_2A_1} = \mathcal{H}^{(k)}_{E_2A_1} = 0,$$
$$\mathcal{H}^{(k)}_{E_2B_1} \propto \begin{pmatrix} -k_y \\ k_x \end{pmatrix}, \quad \mathcal{H}^{(k)}_{E_2B_2} \propto \begin{pmatrix} k_x \\ k_x \end{pmatrix},$$
$$\mathcal{H}^{(k)}_{E_2E_1} \propto \begin{pmatrix} k_y & k_x \\ k_x & -k_y \end{pmatrix}, \quad \mathcal{H}^{(k)}_{E_2E_2} = 0, \tag{B·13}$$
$$\mathcal{H}^{(\zeta)}_{E_2A_1} = \mathcal{H}^{(\zeta)}_{E_2A_2} = \mathcal{H}^{(\zeta)}_{E_2B_1} = \mathcal{H}^{(\zeta)}_{E_2B_2} = 0,$$
$$\mathcal{H}^{(\zeta)}_{E_2E_1} = 0, \quad \mathcal{H}^{(\zeta)}_{E_2E_2} \propto \begin{pmatrix} 0 & 1 \\ -1 & 0 \end{pmatrix}. \tag{B·14}$$

B.2 C_{4v}

Next, we consider the C_{4v} point group. The C_{4v} point group consists of $\{1, 2C_4, C_2, 2\sigma_x, 2\sigma_d\}$, and allows for one 2d IRR (E) and four 1d IRRs (A_1, A_2, B_1, and B_2). Let us consider a doubly degenerate E mode at the Γ point as the unperturbed state. The unitary representation matrices of these IRRs are given by

$$D_E(C_4) = \begin{pmatrix} 0 & -1 \\ 1 & 0 \end{pmatrix}, \quad D_E(\sigma_x) = \begin{pmatrix} -1 & 0 \\ 0 & 1 \end{pmatrix},$$
$$D_E(C_2) = \begin{pmatrix} -1 & 0 \\ 0 & -1 \end{pmatrix}, \quad D_E(\sigma_d) = \begin{pmatrix} 0 & 1 \\ 1 & 0 \end{pmatrix}, \tag{B·15}$$
$$D_{A_1}(A) = 1 \ (\forall A \in C_{4v}), \tag{B·16}$$
$$D_{A_2}(A) = \begin{cases} 1 & \text{for } A = C_4, C_2 \\ -1 & \text{for } A = \sigma_x, \sigma_d \end{cases}, \tag{B·17}$$
$$D_{B_1}(A) = \begin{cases} 1 & \text{for } A = C_2, \sigma_x \\ -1 & \text{for } A = C_4, \sigma_d \end{cases}, \tag{B·18}$$
$$D_{B_2}(A) = \begin{cases} 1 & \text{for } A = C_2, \sigma_d \\ -1 & \text{for } A = C_4, \sigma_x \end{cases}. \tag{B·19}$$

Using a similar symmetry argument to the C_{6v} case, relevant matrix elements are written as

$$\mathcal{H}^{(k)}_{EE} = 0, \quad \mathcal{H}^{(k)}_{EA_1} \propto \begin{pmatrix} k_x \\ k_y \end{pmatrix}, \quad \mathcal{H}^{(k)}_{EA_2} \propto \begin{pmatrix} -k_y \\ k_x \end{pmatrix},$$
$$\mathcal{H}^{(k)}_{EB_1} \propto \begin{pmatrix} k_x \\ -k_y \end{pmatrix}, \quad \mathcal{H}^{(k)}_{EB_2} \propto \begin{pmatrix} k_y \\ k_x \end{pmatrix}, \tag{B·20}$$
$$\mathcal{H}^{(\zeta)}_{EE} \propto \begin{pmatrix} 0 & 1 \\ -1 & 0 \end{pmatrix},$$
$$\mathcal{H}^{(\zeta)}_{EA_1} = \mathcal{H}^{(\zeta)}_{EA_2} = \mathcal{H}^{(\zeta)}_{EB_1} = \mathcal{H}^{(\zeta)}_{EB_2} = 0. \tag{B·21}$$

From the above equations, we immediately find that the first-order term in $\boldsymbol{k}$ and the cross term between $\boldsymbol{k}$ and ζ vanish. It is also clear that $\mathcal{H}^{(\zeta)} \propto \sigma_2$ and $\mathcal{H}^{(\zeta^2)} \propto \hat{1}$. As for the second-order term in $\boldsymbol{k}$, we have

$$\mathcal{H}^{(k^2)} = c_0|\boldsymbol{k}|^2 + c_{A_1}\begin{pmatrix} k_x^2 & k_xk_y \\ k_xk_y & k_y^2 \end{pmatrix} + c_{A_2}\begin{pmatrix} k_y^2 & -k_xk_y \\ -k_xk_y & k_x^2 \end{pmatrix} + c_{B_1}\begin{pmatrix} k_x^2 & -k_xk_y \\ -k_xk_y & k_y^2 \end{pmatrix} + c_{B_2}\begin{pmatrix} k_y^2 & k_xk_y \\ k_xk_y & k_x^2 \end{pmatrix}, \tag{B·22}$$

which is cast into Eq. (13).

B.3 C_{3v}

Finally, let us consider the C_{3v} point group. It consists of $\{1, 2C_3, 3\sigma_x\}$ and allows one 2d IRR (E) and two 1d IRRs (A_1 and A_2). The unitary representation matrices of these IRRs are given as follows:

$$D_E(C_3) = \begin{pmatrix} -\frac{1}{2} & -\frac{\sqrt{3}}{2} \\ \frac{\sqrt{3}}{2} & -\frac{1}{2} \end{pmatrix},$$
$$D_E(\sigma_x) = \begin{pmatrix} -1 & 0 \\ 0 & 1 \end{pmatrix}, \tag{B·23}$$
$$D_{A_1}(A) = 1 \ (\forall A \in C_{3v}), \tag{B·24}$$
$$D_{A_2}(A) = \begin{cases} 1 & \text{for } A = C_3 \\ -1 & \text{for } A = \sigma_x \end{cases}. \tag{B·25}$$

Starting with a doubly degenerate E mode in the unperturbed system, we consider its effective Hamiltonian. Using the symmetry constraints Eqs. (A·17) and (A·18), the relevant matrix elements are shown to be

$$\mathcal{H}^{(k)}_{EE} \propto \begin{pmatrix} k_y & k_x \\ k_x & -k_y \end{pmatrix},$$
$$\mathcal{H}^{(k)}_{EA_1} \propto \begin{pmatrix} k_x \\ k_y \end{pmatrix}, \quad \mathcal{H}^{(k)}_{EA_2} \propto \begin{pmatrix} k_y \\ -k_x \end{pmatrix}, \tag{B·26}$$
$$\mathcal{H}^{(\zeta)}_{EE} \propto \begin{pmatrix} 0 & 1 \\ -1 & 0 \end{pmatrix}, \quad \mathcal{H}^{(\zeta)}_{EA_1} = \mathcal{H}^{(\zeta)}_{EA_2} = 0. \tag{B·27}$$

One may wonder whether the linear term in $\boldsymbol{k}$ is available, because the matrix element $\mathcal{H}^{(k)}_{EE}$ is nonzero. However, it must be zero if the two states of "bra" and "ket" in the matrix element are identical.

To prove this property, we must consider the TRS of the unperturbed system. By the complex conjugation of Eq. (A·7) or (A·26), we can see that $(u^{(0p)}_{-\boldsymbol{g}})^*$ satisfies the same equation as $u^{(0p)}_{\boldsymbol{g}}$. Therefore, we have

$$(u^{(0p)}_{-\boldsymbol{g}})^* = \sum_{q=1,2} u^{(0q)}_{\boldsymbol{g}} U_{qp}, \tag{B·28}$$

for the unitary matrix U. The compatibility between Eqs. (A·8) and (B·28) implies that

$$D_R(A) = U D^*_R(A) U^\dagger. \tag{B·29}$$

In our formulation, $D_R(A)$ is taken to be real. Therefore, by Schur's lemma, such U is only a phase factor. On the other hand, by complex conjugation of Eq. (A·12) or (A·28) with the aid of Eq. (B·28), we find

$$(\mathcal{H}^{(k)}_{pq})^* = -[U^\dagger \mathcal{H}^{(k)} U]_{pq} = -\mathcal{H}^{(k)}_{pq}. \tag{B·30}$$

That is, the first-order term in $\boldsymbol{k}$ is pure imaginary. According to the symmetry argument along with the hermiticity of the effective Hamiltonian, $\mathcal{H}^{(k)}_{pq}$ must be written as $c(k_x\sigma_1 + k_y\sigma_3)_{pq}$ with a real coefficient c. This is definitely real and is contradictory to the purely imaginary $\mathcal{H}^{(k)}_{pq}$. To prevent this contradiction, $\mathcal{H}^{(k)}_{pq}$ must be zero.

Using the matrix elements involving the intermediate states, the second-order term in $\boldsymbol{k}$ becomes

$$\mathcal{H}^{(k^2)}_E = (c_0 + c_E)|\boldsymbol{k}|^2\hat{1} + c_{A_1}\begin{pmatrix} k_x^2 & k_xk_y \\ k_xk_y & k_y^2 \end{pmatrix}$$

$$+ c_{A_2} \begin{pmatrix} k_y^2 & -k_x k_y \\ -k_x k_y & k_x^2 \end{pmatrix}, \qquad \text{(B·31)}$$

which is cast into Eq. (13). The first- and second-order terms in ζ are proportional to σ_2 and $\hat{1}$, respectively. In contrast to that in the C_{6v} and C_{4v} cases, the cross term between $\boldsymbol{k}$ and ζ in the C_{3v} case survives. It is generally written as $\mathcal{H}^{(k\zeta)} = k_x C_x + k_y C_y$ with the 2×2 hermite matrices C_x and C_y. By applying $A = \sigma_x$ in Eq. (9), the off-diagonal elements of C_x and the diagonal elements of C_y vanish. Subsequently, we apply $A = C_3$, resulting in Eq. (16). These forms of the effective Hamiltonian are consistent with the TRS, i.e., Eq. (B·28), of the unperturbed system.

1) D. B. Kaplan: Phys. Lett. B **288** (1992) 342 .
2) S. Y. Zhou, G. Gweon, A. V. Fedorov, P. N. First, W. A. de Heer, D. Lee, F. Guinea, A. H. Castro Neto, and A. Lanzara: Nat. Mater. **6** (2007) 770.
3) R. Jackiw and C. Rebbi: Phys. Rev. D **13** (1976) 3398.
4) G. W. Semenoff: Phys. Rev. Lett. **53** (1984) 2449.
5) Y. Hatsugai: Phys. Rev. Lett. **71** (1993) 3697.
6) F. D. M. Haldane and S. Raghu: Phys. Rev. Lett. **100** (2008) 013904.
7) Z. Wang, Y. D. Chong, J. D. Joannopoulos, and M. Soljačić: Phys. Rev. Lett. **100** (2008) 013905.
8) Y. D. Chong, X. G. Wen, and M. Soljačić: Phys. Rev. B **77** (2008) 235125.
9) G. E. Volovik: *The Universe in a Helium Droplet* (Oxford University Press, New York, 2009) p. 138.
10) X.-L. Qi, T. L. Hughes, S. Raghu, and S.-C. Zhang: Phys. Rev. Lett. **102** (2009) 187001.
11) M. Sato and S. Fujimoto: Phys. Rev. B **79** (2009) 094504.
12) F. D. M. Haldane: Phys. Rev. Lett. **61** (1988) 2015.
13) If the magnetic flux per unit cell is a fractional (q/p for co-prime p and q) multiple of the flux quantum, the problem becomes a Hofstadter one. In this case, the momentum $\boldsymbol{k}$ is still a good quantum number however, the Brillouin zone is reduced by factor p.
14) M. V. Berry: Proc. Roy. Soc. (Lond.) A **392** (1984) 45.
15) T. Ochiai: Phys. Rev. B **86** (2012) 075152.
16) X.-L. Qi and S.-C. Zhang: Rev. Mod. Phys. **83** (2011) 1057.
17) M. Plihal and A. A. Maradudin: Phys. Rev. B **44** (1991) 8565.
18) D. Cassagne, C. Jouanin, and D. Bertho: Phys. Rev. B **53** (1996) 7134.
19) M. Onoda, S. Murakami, and N. Nagaosa: Phys. Rev. E **74** (2006) 066610.
20) K. Ohtaka, T. Ueta, and K. Amemiya: Phys. Rev. B **57** (1998) 2550.
21) K. Ohtaka, J. Inoue, and S. Yamaguti: Phys. Rev. B **70** (2004) 035109.
22) T. Ochiai and M. Onoda: Phys. Rev. B **80** (2009) 155103.
23) F. Zhang, A. H. MacDonald, and E. J. Mele: Proc. Natl. Acad. Sci. USA **110** (2013) 10546.
24) K. S. Novoselov, E. McCann, S. V. Morozov, V. I. Fal'Ko, M. I. Katsnelson, U. Zeitler, D. Jiang, F. Schedin, and A. K. Geim: Nat. Phys. **2** (2006) 177.
25) D. M. Pozar: *Microwave Engineering* (Wiley, 2005) 3rd ed., Chap. 9.
26) T. Inui, Y. Tanabe, and Y. Onodera: *Group Theory and its Applications in Physics* (Springer-Verlag, Berlin, 1996) Appendix B.